Case Studies in Thermal Engineering 41 (2023) 102513

Contents lists available at ScienceDirect

Case Studies in Thermal Engineering

journal homepage: www.elsevier.com/locate/csite

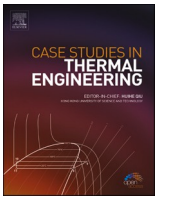

Numerical and experimental investigation on the effect of heat release rate in the evolution of fire whirls

Alexis Cantizano [a,b,*], Pablo Ayala [a,b], Eva Arenas [a,b], José Rubén Pérez [b], Cándido Gutiérrez-Montes [c]

[a] Institute for Research in Technology, ICAI, Comillas Pontifical University, c/ Sta. Cruz de Marcenado, 26, 28015, Madrid, Spain
[b] ICAI School of Engineering, Comillas Pontifical University, c/ Alberto Aguilera, 25, 28015, Madrid, Spain
[c] Fluid Dynamics Division of the Department of Mining and Mechanical Engineering, Universidad de Jaén, Campus de las Lagunillas s/n, 23071, Jaén, Spain

ARTICLE INFO

Keywords:
Fire whirl
Heat release rate
Atrium
Full-scale experiments
FDS
Intrusive measurements

ABSTRACT

Buildings with large internal spaces, such as vertical shafts or atria, are widespread nowadays. In the case of fire, internal air currents may generate devastating fire whirls that can cause severe damage due to intensive heat release rate (HRR) and temperatures. This work presents the generation and evolution of fire whirls in a full-scale atrium experiment and their comparison with a numerical approach. A set of numerical models using FDS 6.7.5 are tested to assess the influence of the HRR curve and the impact of intrusive methods of temperature measurements on the prediction of whirls. The results show that the Burgers vortex model is well reproduced, although the continuous flame and plume regions can only be distinguished with fine grids. However, the periodic evolution of the whirls is better predicted with a time-averaged HRR curve, showing its influence on the flame height. The use of the experimental HRR curve presents more accurate results only in the temperatures far from the flame, with errors lower than 8.5% even for coarse grids. In addition, a small obstacle above the flame is observed to affect the formation of the whirls, which consequently impacts the grid sensitivity and computational cost.

Nomenclature

k	Constant of Burgers vortex (m^{-2})
r	Radial distance (m)
r_o	Maximum tangential velocity radial distance (m)
r_T	Temperature core radius (m)
u_θ	Tangential velocity (m/s)
$u_{\theta m}$	Maximum tangential velocity (m/s)
D^*	Characteristic diameter of the plume
P_{amb}	Ambient Pressure (Pa)
T	Temperature (K)
T_{amb}	Ambient temperature (K)

* Corresponding author. Institute for Research in Technology, ICAI, Comillas Pontifical University, c/ Sta. Cruz de Marcenado, 26, 28015, Madrid, Spain.
E-mail address: alexis.cantizano@comillas.edu (A. Cantizano).

https://doi.org/10.1016/j.csite.2022.102513
Received 24 August 2022; Received in revised form 7 October 2022; Accepted 22 October 2022
Available online 27 October 2022

ΔT_m	Maximum excess temperature (K)
Δ	Element size (m)
Γ_0	Circulation (m^2/s)

1. Introduction

The current trend in the construction of high-rise buildings with complex designs and innovative architecture constantly challenges the analysis of possible risks. Large inner spaces, like vertical shafts, atrium, and spiral staircases, are widespread, and circulation currents may be formed due to airflow entrainment. In case of fire, devastating swirling can be generated, as has been already observed in recent high-rise fire incidents, like the Beijing Television Cultural Center and Plasco Building [1]. Fire whirls are concentrated vortex structures that release high amounts of heat, which causes spotting fire, and accelerates fire spread significantly [2]. Although these fire whirls may remain stable over a brief time, they can cause human fatalities and severe damage [3].

They have been broadly investigated using burners, small-scale pools and gaseous fuel fire whirls, with research mainly focused on their quasi-steady behaviour. Different types of facilities have been used, like fixed-frame facilities where the airflow enters the test region tangentially [4–11] and rotating screen types [12–15], where an advantageous control of the circulation strength can be varied through adjustment of the angular velocity of the screen. However, the experimental methods present some inevitable limitations, such as the use of intrusive measuring techniques that may alter the flow dynamics or the flame behaviour. Temperature is generally measured in fixed thermocouple trees and flow velocity with bidirectional venturi tubes [1], located at a discrete number of specific locations. Moreover, the accuracy of non-intrusive methods, like optical-based measuring techniques, highly depends on optical properties, which are challenging to acquire [16].

Numerical models have also been widely developed as a fundamental approach to understanding the whirls' behaviour. The first experiments of fire whirls [17] were numerically modelled with Fire Dynamics Simulator (FDS) in Ref. [18]. They carried out Large Eddy Simulations (LES) with a fixed fire strength and a variable circulation to understand the plume dynamics and combustion. However, they highly recommended further research on a variable heat release rate input to their models. Also, the influence of the vent conditions on the possible appearance of fire whirls within atria was analysed with Fluent in Ref. [19]. Later, Snegirev et al. [20] conducted CFD simulations and experiments in an asymmetric medium-scale compartment, obtaining an unsteady fire whirl characterised by its periodic formation and consecutive destruction and flame precession. This flame precession, which increases the difficulty of experimental measuring, could expand the intense burning area and cause more damage [21].

Due to randomly distributed flame sources in natural circumstances, spontaneous fire whirls were firstly simulated in Ref. [22]. They proved that the interaction effects among multiple flame sources caused the formation of fire whirls. Later, Zhou [23] proposed a method for spontaneous fire whirl analysis and prediction due to non-regularly distributed flame sources, supported by numerical simulations with FDS. The authors provided an adapted criterion based on an equivalent gap fraction, which could assess real fire disasters and could allow the prevention of fire whirls.

In addition, most studies of fire whirls generation within buildings are focused on the vertical shafts of tall buildings [24–26]. These studies mainly focus on evaluating the flame's height, shape, and velocity fields through theoretical analysis and experimental comparison. Recently, Yan et al. [10] numerically studied the fire whirl development in a medium-scale fixed-frame facility to satisfactorily propose a hybrid swirling vector and tangential velocity refinement approach to precisely identify their vortex cores.

The present work analyses the generation of fire whirls in an atrium where the inlet air enters as in a fixed-frame facility. However, compared to that, the outer walls are at a much larger distance with respect to the fire location. The influence of the measured heat release rate (HRR) as input data on the numerical models with FDS 6.7.5. is assessed. The numerical prediction of the evolution of whirls generated from a pool fire under cross-ventilated conditions is clearly affected by the measured intensifications of HRR. A time-averaged HRR allows more accurate results, despite the far-field temperatures are underpredicted, allowing the evaluation of different possible fire scenarios. In addition, the intrusive way of measuring temperatures in these types of full-scale experiments is also numerically verified to impact the formation of whirls, affecting the definition of the models in terms of computational cost.

The paper is arranged as follows: a brief description of the experimental setup and tests conditions are initially presented, followed by the definition of the numerical models. Then, a description of how fire whirls can be numerically characterized is made. Subsequently, numerical results are compared with the experimental measurements and assessed with different ways of introducing the heat release rate. The influence of the HRR nominal value is also numerically evaluated and finally, the last section is devoted to the conclusions.

Table 1
Fire experiments and time-averaged HRR.

Test	Pan diameter (m)	Heptane weight (kg)	HRR (MW)	T_{amb} (°C)	P_{amb} (Pa)
1	1.17	36	2.66	21.5	101,651
2	0.92	29	1.54	20.1	101,651

2. Materials and methods

2.1. Experimental setup

The fire experiments were conducted in the Fire Atrium of Murcia, Spain [27–29] and their main characteristics are outlined in Table 1.

The Fire Atrium is a 19.5 m × 19.5 m × 19.5 m facility (Fig. 1a) with a pyramidal-shaped roof of thin steel walls. The pool fires were placed at the centre of the ground, with the pans filled with heptane, over a thin layer of water. The time-averaged HRRs were evaluated by the fuel mass loss rate measured with three load cells placed underneath the pan. A constant mechanical exhaust of 18.32 m^3/s was generated by only two of the four fans at the central section of the roof. Two air inlet vents of 4.88 m × 2.5 m were opened at the atrium base in an asymmetric layout.

As can be seen in Fig. 1b, two existing horizontal cables of 8 cm diameter crossed the central section of the atrium at different heights. These cables were used to locate some of the thermocouples, and the flame reached only the cable located at the height of 5.1 m. The thermocouples were used to measure the temperature in the fire plume and near the walls.

2.2. Numerical models

Numerical simulations have been carried out with Fire Dynamic Simulator (6.7.5) [30]. The models used to account for combustion, turbulence, and radiation were the Eddy Dissipation Concept (EDC) with a thermal extinction model, the Deardorff model ($C_v = 0.1$) and the radiation transport equation with 100 radiation angles, respectively. The pool fires have been simulated firstly by introducing the experimental HRR values estimated from the measured mass loss rate curves, with a radiation fraction for the heptane of 0.35 [31]. Additionally, the time-averaged HRR curves are also assessed.

The numerical model of the atrium geometry defines the make-up air inlets as open vents. Extended domains at the inlet vents are required to precisely predict the inner fire-induced conditions with circular flow patterns [32]. Thus, two extensions of 3.2 m × 22.6 m × 5.0 m upstream of the inlets are added to the atrium geometry. A constant exhaust flow rate has been introduced at the fan locations, and the external conditions are set as a quiescent atmosphere.

The analysis of the influence of the HRR curve is coupled to a grid sensitivity study only for Test 1, since the influence of the whirls, both in the far and near fields, is expected to be larger than Test 2. For the Large Eddy Simulation (LES) method, a spatial resolution between $5 < D^*/\Delta < 20$ is recommended, where D^* is the characteristic diameter of the plume, and Δ is the element size. To properly analyse the element size influence on the fire whirls generation, three different element sizes in the flame region have been chosen. Considering the time-averaged HRR value of 2.66 MW ($D^* = 1.42$), the coarsest grid corresponds to a simple model with a constant element size of $\Delta = 0.2$ m, which gives a spatial resolution of 7. Then, the medium grid is obtained with an element size of $\Delta = 0.1$ m, only defined in a central prism of dimensions 6 m × 6 m from the bottom to the top of the atrium. And finally, in the finest grid a smaller element size of $\Delta = 0.05$ m has been specifically defined near the flame and in the fire plume, i.e. a central prism of 3 m × 3 m from the bottom to the top of the atrium, surrounded by a region with elements of $\Delta = 0.1$ m up to a distance of 6 m from the centre, and then a region of $\Delta = 0.2$ m up to the external walls.

As aforementioned above, due to the observed whirls formation and their interaction with one of the existing cables at the Fire Atrium, two numerical models were defined: with and without the cable. The cable is positioned at 9.75 m from the walls with the inlets, and at a height of 5.1 m. The grid resolution influences the cable thickness assumed in the simulations, and thus, to compare with all the models, a constant thickness of 0.2 m has been used. With the finest grid, two other thicknesses have been evaluated for the central section: 0.1 m and 0.05 m.

The total number of elements for the coarsest, medium and finest grids are 1,025,282, 1,964,416, and 3,737,432 respectively. Finally, it is essential to note the computational cost of the simulations. They all have been completed in a multi-parallel process, with a noticeable difference between them (Table 2).

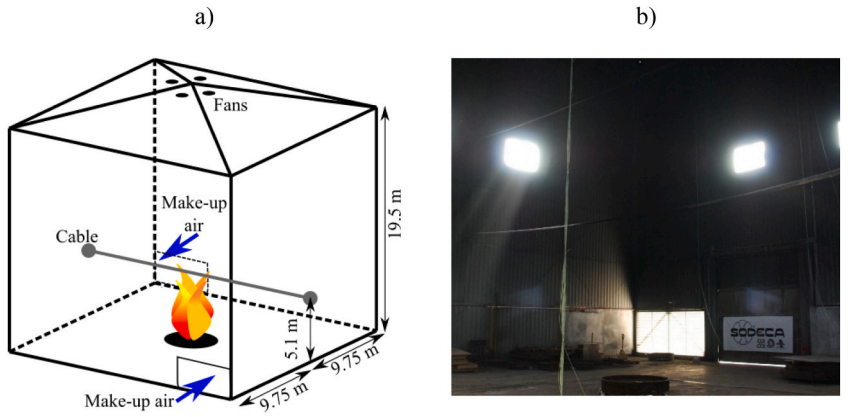

Fig. 1. a) Fire experiment layout and b) indoor photography of the Fire Atrium.

Table 2
Computational cost of the numerical models (Test 1).

	N° of cores	N° elements	Computational cost (h)	
			No cable	Cable
$\Delta = 0.2$ m	11	1,025,282	12.5	12.8
$\Delta = 0.1$ m	11	1,964,416	58.7	58.6
$\Delta = 0.05$ m	13	3,737,432	134.0	141.8

2.3. Fire whirls characterisation

Circulation is the key factor that characterises fire whirls, as the velocity and temperature fields depend on it. Also, the flame height can be considered a function of circulation. In liquid pool fires, the base part of the flame approaches the pool due to the radial imbalance of pressure gradient and the reduced centrifugal force because of the viscous stresses near the ground, i.e. Ekman-like boundary layer. The heat input to the fuel is then increased, and consequently, the fuel evaporation rate is enhanced, causing significant growth in the flame height [33]. Nevertheless, there are agreed concerns characterising fire whirls over liquid pools, such as the precession of the flame or the heat release rate behaviour [34].

Assuming a constant circulation Γ_0 far from the vortex, the tangential velocity u_θ around a fire whirl is characterised by a Rankine vortex or a Burgers vortex [2], as defined in Equations (1) and (2), respectively.

$$\begin{cases} u_\theta(r) = \left(\dfrac{\Gamma_0}{2\pi r_o^2}\right) r, & r \le r_o \\ u_\theta(r) = \left(\dfrac{\Gamma_0}{2\pi}\right) \dfrac{1}{r}, & r > r_o \end{cases} \tag{1}$$

$$u_\theta(r) = \left(\frac{\Gamma_0}{2\pi r}\right)\left(1 - e^{-kr^2}\right) \tag{2}$$

The radial distance r_o is measured where the maximum tangential velocity $u_{\theta m}$ is reached. In the case of a Burgers vortex, the constant k can be obtained considering that the maximum tangential velocity $u_{\theta m}$ is at:

$$\mathrm{r_o} = 1.1209 k^{-0.5} \tag{3}$$

The vortex is described by an inner viscous core where vorticity is involved and an outer free vortex that lacks vorticity. The transition between the inner and the outer cores is sharp for the Rankine vortex and smooth for the Burgers vortex. The latter is accepted throughout an exhaustive amount of experimental studies to be the best representation of the velocity field of a whirl [4,16,34,35].

Fire whirls have a fuel-rich core with no active combustion reaction. This significantly influences the radial temperature distribution throughout the continuous flame region [11]. The core radius is considered the location where the maximum temperature is achieved. Outside this core, the temperature decreases. Above the intermittent flame region, i.e. the fire plume, the maximum excess temperature ($\Delta T_m = T - T_{amb}$) moves towards the centre of the whirl, behaving as a Gaussian profile. Thus, the temperature core radius r_T is defined, in this case, where the excess temperature is reduced to half of its maximum value.

3. Results and discussion

In this section, for Test 1, the influence of the HRR curve in the fire whirls generation is analysed by studying both the experimentally measured and the time-averaged values with different grid resolutions, Fig. 2. The temperatures in the vicinity of the flame and in the far-field, i.e. near the walls, are assessed. The tangential velocity and the excess temperature behaviours are also evaluated to verify the formation of whirls. Additionally, it is shown how the presence of the lowest cable influences the whirl formation. Finally,

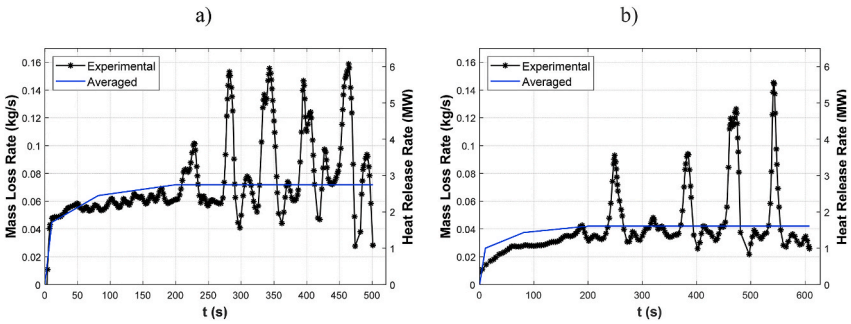

Fig. 2. Measured and time-averaged mass loss rate and HRR curves: a) Test 1; b) Test 2.

for both experimental tests and two additional numerical scenarios, a qualitative numerical analysis of how the time-averaged HRR values affect the predicted whirls is performed.

3.1. Measured heat release rate curves

The heat release rate curves evaluated by the measured mass loss rate and also, for the sake of clarity, the proposed time-averaged curves, are shown in Fig. 2. The latter have been modelled as piecewise linear functions: starting with a value of 0 for the initial time, 62.4% of its time-averaged value at 10.7 s, 89.1% at 81.5 s, and 100% at 200 s. This maximum value remains constant until the end of the fire [36,37].

In Test 1, five main fire whirls were observed, which corresponds to the peaks of the measured heat release rate curve (Fig. 2a). In Test 2, also five whirls were observed (Fig. 2b). However, the second whirl generated, at 320 s after ignition, did not stabilize. A periodic flame wander, self-rotation, around the centreline was observed before the stabilisation of each of the formed fire whirls. For both tests, an average period of 60 s was needed for the generation of every whirl. Then, a self-rotating flame and its simultaneous rotation around the centre of the pool was noticed. During the experiments, the cable influenced the generated fire whirls differently, as shown for Test 1 in Fig. 3a–e and for Test 2 in Fig. 3f–j. The acquired rotation around the centre was reduced, and three different behaviours were observed: the flame was tilted (Fig. 3a–b, f-g), the continuous flame region was interrupted (Fig. 3c–d, h-i), and the height of the flame was enhanced when the contact with the cable was avoided (Fig. 3e, j).

The whirls have been verified by visual inspection, as can be seen in the videos (Test 1: whirl#1_1, whirl#1_2, whirl#1_3, whirl#1_4, whirl#1_5; Test 2: whirl#2_1, whirl#2_2, whirl#2_3, whirl#2_4, whirl#2_5) included in the online version of the paper. They were recorded with a video camera Fujitsu with a frame size of 1980 × 1080 pixels, and 25 frames per second. From them, the flame height of Test 1 cannot be properly assessed because the camera was focused to reach a maximum height of about 6 m. As it can be observed from the videos, this maximum height was exceeded by the flame at some instants, although due to their instabilities this value is relatively close to the end of the flame. For Test 2, the flame height is estimated from video image processing, and the five whirls present averaged heights from 4.1 m to 4.9 m, which correspond with averaged HRRs from 1.9 MW to 2.4 MW and reach maximum heights from 5.5 m to 6.1 m.

The near flame behaviour is always difficult to analyse and compare due to the slow thermal response of the thermocouples and the fast variation of the predicted temperatures obtained from the simulations. However, this numerical-experimental comparison is needed here to account for the fire whirl formation by observing the temperature peaks during the test. The temperature near the flame is measured by a sensor located in the fire plume at the height of 4.6 m. The temperature behaviour of the different whirls is not repeated due to their non-stability and deviations from the central location of the sensor.

As commented above, the following analysis is only performed with Test 1. Thus, focusing on the time interval when the whirls appear, i.e. 200 s–500 s, the numerical results show how the temperature differs from the experimental measurements at this height due to the proximity to the flame (Fig. 4a-b). When the cable is not included, the relevant reduction in the values of the numerically predicted temperature proves how the rotation of the flame around the pan is slower than in the experiment (Fig. 4a). Despite the high values of HRR, and the measured behaviour of periodic straight swirling flames, only a notorious stable and centred fire whirl is noticed, generated at time 463 s with the element size of 0.1 m. With the other two element sizes, some whirls are also predicted, although they are tilted and deviated from the centre. In the simulations with the cable, more repeated peak temperatures are

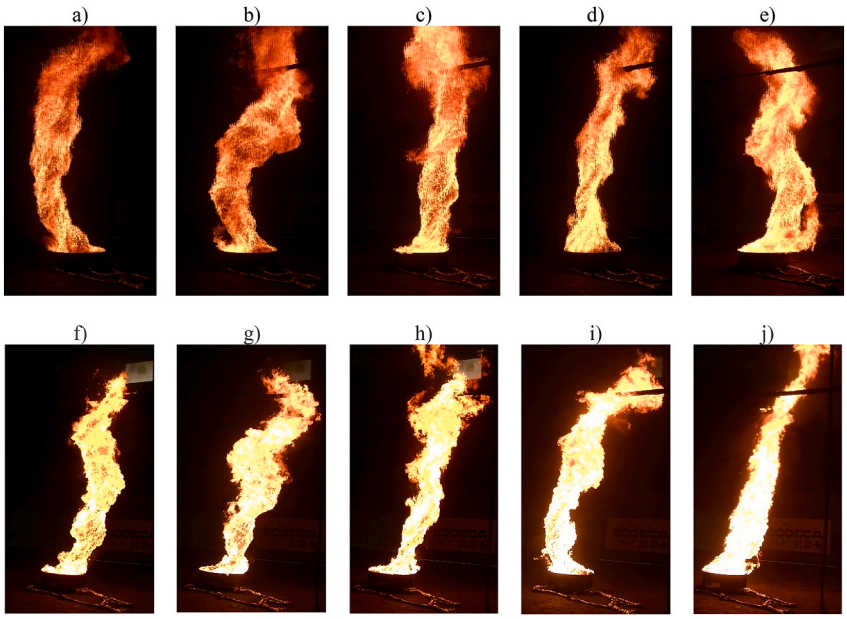

Fig. 3. Fire whirls interaction with the cable: a-e) Test 1; f-j) Test 2.

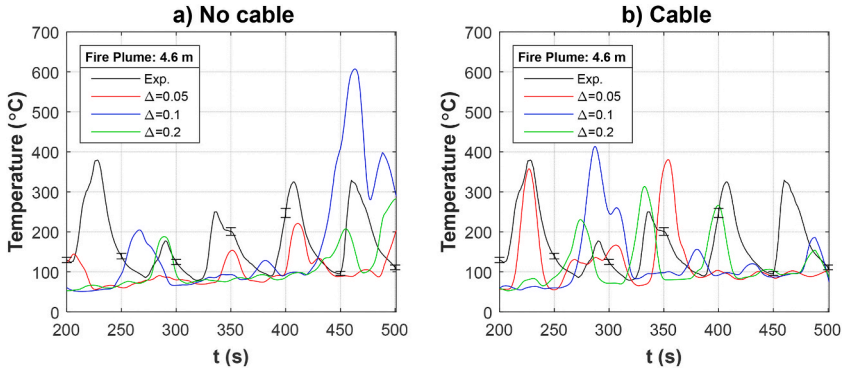

Fig. 4. Numerical-experimental comparison of the temperatures in the near-field.

predicted (Fig. 4b), particularly for the coarsest mesh. In the same way, more unstable but straight flames are developed with the finest grid during the first 400 s. With $\Delta = 0.1$ m, a relevant fire whirl is predicted at 290 s, but its stability is clearly much lower than the one obtained when the cable is introduced. From these results, it can be concluded that the input of the measured HRR data (Fig. 2a) does not guarantee the formation of the fire whirls at the same time instants as in the experiments. Nonetheless, fire whirls are also numerically generated, as will be proved by the evaluation of the tangential velocity and radial excess temperature behaviour in Fig. 5.

The azimuthal or tangential velocity and the excess temperature are evaluated to numerically assess the fire whirl behaviour for those instants with a peak temperature in the near-field. The models without the cable are only considered to obtain a better estimation

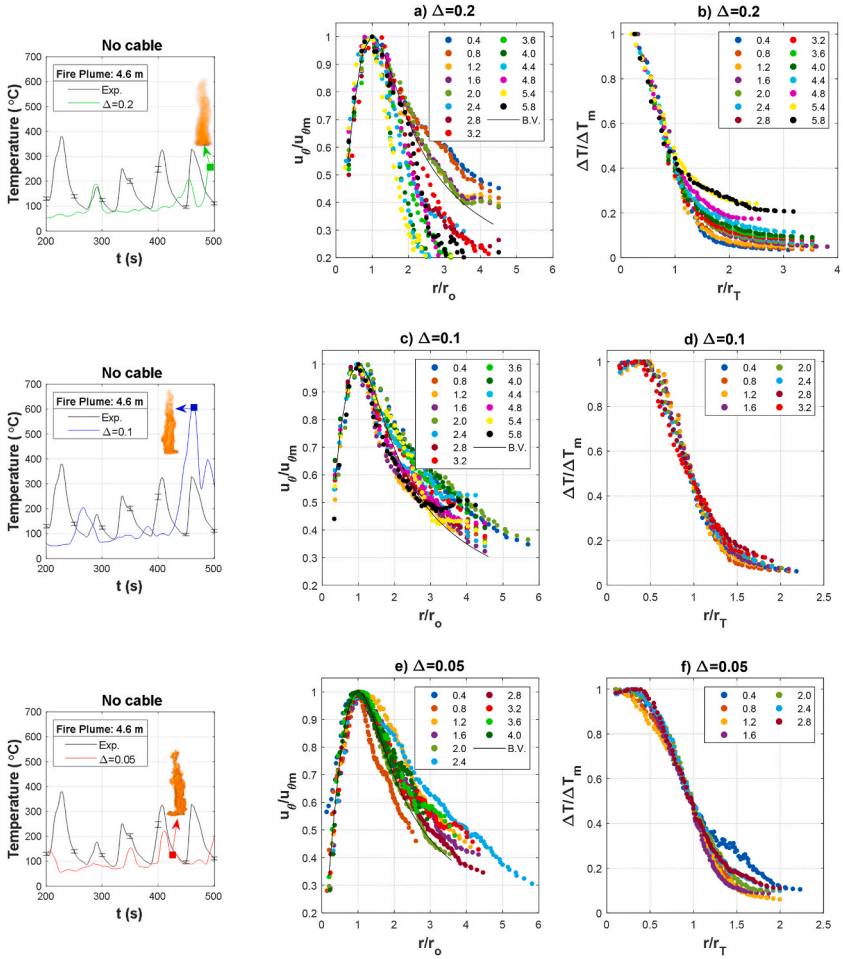

Fig. 5. Normalised tangential velocity and excess temperature at different heights.

of the maximum height that the whirls can reach, Fig. 5. The ratio of the tangential velocity with respect to the maximum value $(u_\theta / u_{\theta m})$ is represented at different heights as a function of the normalised radial distance (r/r_o). These curves are compared with the theoretical Burgers vortex model (denoted as B.V.), where the parameter k has been obtained for an averaged r_o calculated from the values evaluated at every height (Fig. 5a, c, e). The ratio of the excess temperature (ΔT) and the maximum excess temperature (ΔT_m) is also shown as a function of the normalised radial distance (r/r_T) for different heights (Fig. 5b, d, f). It has to be mentioned that for every element size, only one fire whirl has been represented. The corresponding time instants are 493 s, 464 s and 426 s for the element sizes of 0.2 m, 0.1 m and 0.05 m, respectively.

The tangential velocity reproduces well the Burgers vortex for each of the three meshes, with a duration of a few seconds. With the coarsest grid (Fig. 5a), it can be observed how the tangential velocity is reduced gradually, with respect to the maximum value, as the height increases. The temperatures behave with the same trend for all the heights, which does not allow to distinguish the continuous flame region from the plume region, i.e. the maximum temperature seems to be at the centre of the whirl. For the other two numerical models with a higher density of the grid, the tangential velocity shows a closer approach to the theoretical curve. For $\Delta = 0.1$ m, the Burgers vortex is rather followed up to a height of 5.8 m (Fig. 5c). However, the predicted temperatures corroborate this only up to the height of 3.2 m (Fig. 5d). The excess temperature behaviour clearly shows the two regions, i.e. the continuous flame and the plume. But for the sake of clarity, only the former region is represented, noticing that the maximum temperature is not located at the centre of the whirl. With the finest grid, u_θ reproduces the averaged theoretical curve only up to the height of 4.0 m (Fig. 5e). In the same way, the continuous flame region is shorter, reaching a height of 2.8 m (Fig. 5f). It is important to note that the results herein evaluated correspond to different values of HRR, as for every grid size, the most relevant whirls were not generated according to the highest values of the measured HRR values. The tangential velocity fields with their temperature core radius for the same fire whirls are represented in Fig. 6. The heat release rate values correspond to 4.8 MW, 7.3 MW and 3.6 MW for the element sizes of 0.2 m, 0.1 m and 0.05 m, respectively. As previously commented, the whirl is not well predicted with the coarsest grid, as both the maximum tangential velocity and the temperature are below the expected values. The maximum tangential velocity and temperature are similar to the other two smaller element sizes. In the case of the $\Delta = 0.1$ m, the HRR introduced is very high, which substantially increases the temperature core radius. With the finest grid, the predicted whirl centre is at the farthest distance from the central axis of the atrium base, as can be noticed by the small temperature rise (Fig. 4a).

The influence of the fire whirls on the smoke production can be studied by comparing the temperature in the far field. The far-field behaviour is assessed by the temperature measured at 30 cm away from the walls, at heights of 7.5 m and 15.0 m. The results obtained with both models, with and without the cable, show that neither the element size nor the cable has an impact on the gas temperature at these locations. The temperature increases smoothly as time grows and the numerical predictions can be all considered to be within the expected uncertainty for the three numerical models. The maximum temperatures achieved are shown in Table 3, reaching a maximum relative error lower than 8.5%.

The previous results indicate that both numerical models, with and without the cable, properly predict the temperature behaviour of the far field. This is useful when defining the smoke behaviour and filling of this large volume. Thus, the coarsest grid is a reasonable choice and relatively fast. But only with smaller element sizes fire whirls are properly predicted, or at least, the flame behaviour is closer to the experimental observations. Nonetheless, due to the continuous variation of the HRR input, the generated fire whirls become more unstable with respect to time. The computational cost for these finer grids is a major concern when defining the numerical models of these types of fire scenarios. In addition, a small obstacle related to the intrusive temperature measurement methods may affect the inner conditions' results, which increases the computational cost for the most refined grid (Table 2). When modelling the cable, the number of numerical straight fire whirls seems to increase, and the results are closer to the observed behaviour during the experiment.

3.2. Time-averaged HRR

For Test 1, six numerical models with a time-averaged HRR value are carried out, with and without the cable, and with the same element sizes as in the previous section.

The temperatures in the near-field, obtained for the sensor located in the fire plume at 4.6 m high, are shown in Fig. 7. The lack of HRR peaks in the time-averaged HRR clearly influences the temperatures obtained during the flame wander or flame revolution around the pan. In the simulations with the cable, and particularly with the coarsest grid, fire whirls are not really appreciated except for the one generated at 428 s (Fig. 7b). With $\Delta = 0.1$ m, the predicted temperatures can be considered quite reliable for the models

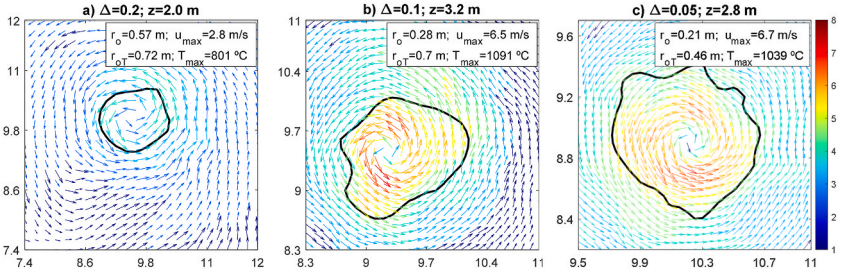

Fig. 6. Tangential velocity fields and temperature core radii.

Table 3
Maximum temperatures in the far-field (Test 1).

Height		Temperature (°C)/Error (%)			
		Exp.	$\Delta = 0.2$	$\Delta = 0.1$	$\Delta = 0.05$
7.5 m	No cable	98.6	105.6/7.0	104.0/5.5	98.2/0.4
	Cable		104.0/5.5	93.9/4.8	92.7/6.0
15 m	No cable	109.1	114.5/5.0	118.4/8.5	105.9/2.9
	Cable		116.3/6.6	110.1/0.9	99.9/8.4

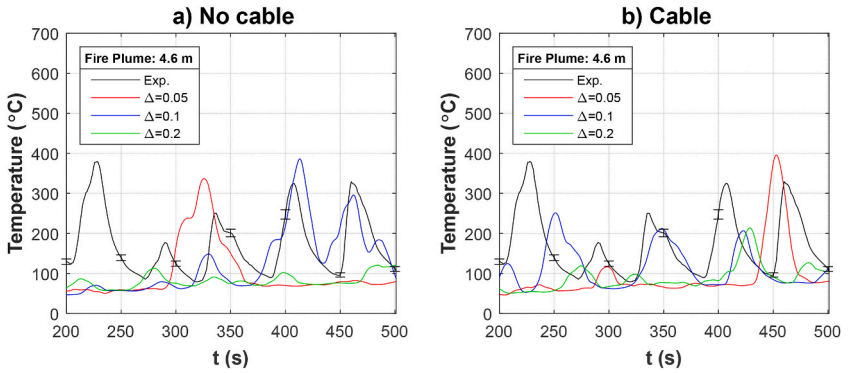

Fig. 7. Temperature near the flame with an averaged value of the HRR.

without and with the cable, after 350 s and 250 s, respectively. As can be seen in both models, with this element size, the frequency of their generation is reproduced with fairly good precision. Finally, for the most refined grid, the temperature is underpredicted as a consequence of the flame rotation around the pan. Only one centred and straight fire whirl is generated during the complete simulation for both numerical models. It has to be mentioned that when considering the cable, this fire whirl is less stable, as was observed in the experiments.

Therefore, the results obtained with $\Delta = 0.1$ m seem to be reasonably reliable when assessing the temperatures in the near-field. However, with this size, the flame does not reach the cable, mainly due to the smaller value of the introduced time-averaged HRR value. This can be easily verified, in the numerical model with the cable, for the observed last whirl (421 s), which is the numerically most noticed in terms of circulation, as can be observed by the absolute value of the tangential velocity at different heights (Fig. 8.). An almost constant circulation is obtained up to a height of 2.4 m. At higher locations, the circulation starts to vanish, and the velocity begins to decrease at 3.2 m high.

Despite the higher discrepancy in the temperatures obtained with $\Delta = 0.05$ m, the height reached by the fire whirls is much more realistic when compared with the experiments (Fig. 3.). Again, in the numerical model with the cable, this height is deduced by the normalised tangential velocity and radial excess temperature represented in Fig. 9. When the whirl does not interact with the cable (456 s), the Burgers vortex is precisely predicted up to a height of 4.4 m (Fig. 9a). In the same way, the height of the whirl can be distinguished by the continuous flame region which reaches a height of 3.2 m. These results are quite similar to those obtained in the previous section for the same element size.

The velocity vortex is affected by the proximity of the cable, as its centre is observed to be far from the location of the pool as the height increases. Moreover, the tangential velocity is higher than expected for $r > 2r_o$ (Fig. 9.), mainly because of a slower deceleration of the flow around the inner core. Values of the tangential velocity greater than 10 m/s are obtained in the simulations.

In Fig. 10, different instants of the numerical fire whirl can be observed. As commented above, when the inner core is not aligned with the pan centre, the height of the flame reached is above the cable. However, for the periods of time when it is centred, the

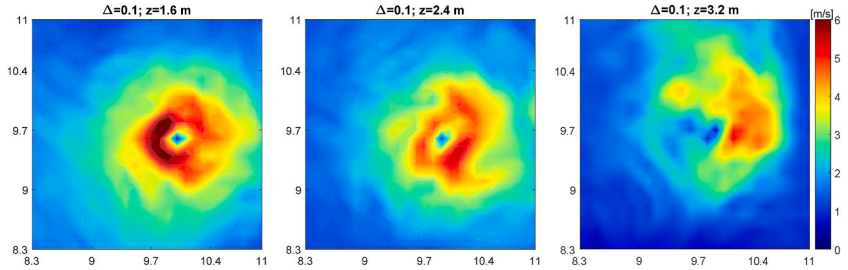

Fig. 8. Tangential velocity at different heights; with cable and for $\Delta = 0.1$ m (421 s).

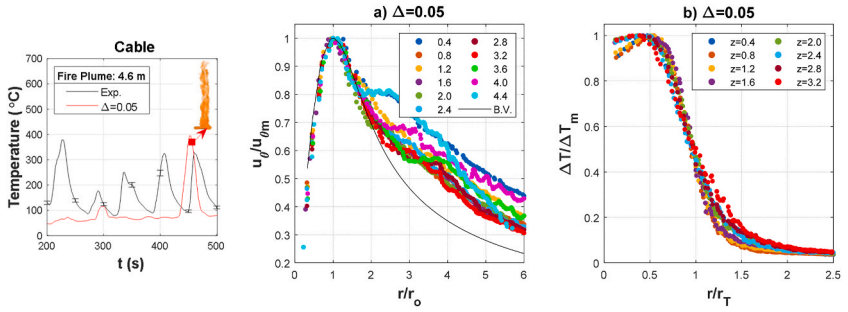

Fig. 9. Normalised tangential velocity and excess temperature at different heights.

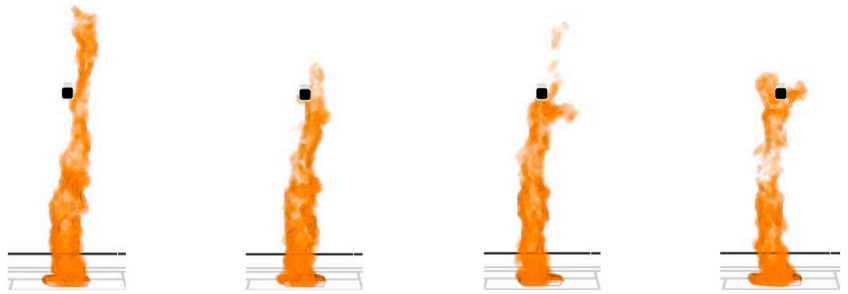

Fig. 10. Numerical fire whirls; with cable and $\Delta = \mathbf{0.05}$ m.

influence of the cable is notable. The numerical model reproduces well some of the behaviours described in Fig. 3.

A further refinement in the thickness of the cable is also assessed. In the finest grid, two other thicknesses for the central section are considered, i. e. 0.1 m and 0.05 m. Only one single straight fire whirl was formed for every model, and their duration was similar to those predicted in the previous model with the cable (Fig. 7b) and also as it was observed during experiments. It has to be highlighted that when the cable is not introduced in the numerical models, more stable straight whirls are predicted with this grid resolution. This confirms the need to introduce small obstacles that may interact with swirling flames, although their definition depends on the sensitivity of the mesh and the computational cost that can be afforded.

Finally, to assess the numerical performance of the model in the far-field, temperatures in the sensors located at 7.5 m and 15 m high close to the wall are again analysed. The numerical results follow the increasing trend of the measured temperatures up to 350 s with differences lower than 5%. Then, the predicted growth diminishes, with the temperatures being underpredicted. In Table 4, the final temperatures can be seen with a maximum error of 17.7% for the finest grid. As the HRR is equivalent to the previous case, this change might be explained by the decrease in the turbulence produced by smaller whirls ($\Delta = 0.1$ m) or by the formation of a lesser number of whirls ($\Delta = 0.05$ m), as shown in Fig. 7.

Time-averaged heat release rates allow the simulation of more stable fire whirls, but the already known increase in the heat release rate is not introduced. Thus, fire whirls are weaker, and the possible turbulence that can generate may reduce the amount of smoke production. This means that the far-field temperatures can also be influenced. This analysis also proves the impact of the intrusive methods in the experiments and in the numerical models.

These results highlight that special attention should be paid to the mesh resolution when performing numerical assessments of fire scenarios within large spaces with possible circular currents. Coarser grids are useful in performing analysis of smoke behaviour. However, when considering fire spread related to elongated fire whirls, fine grids should be considered, despite the increase in the computational cost of the models. In this regard, although the transient evolution of fire whirls generation might not be well captured, their impact in the near field is properly predicted.

Table 4
Maximum temperatures in the far-field (Test 1).

		Temperature (°C)/Error (%)			
Height		Exp.	$\Delta = 0.2$	$\Delta = 0.1$	$\Delta = 0.05$
7.5 m	No cable	98.6	89.8/8.9	88.2/10.6	80.3/18.6
	Cable		89.0/9.7	90.3/8.4	81.1/17.7
15 m	No cable	109.1	94.8/13.1	101.7/6.7	95.0/12.9
	Cable		95.7/12.3	97.5/10.6	90.2/17.3

3.3. Influence of the HRR nominal value

Following the results from the previous grid analysis, an element size of $\Delta = 0.1$ m is chosen to assess the influence of the HRR nominal value when simulating the four fire scenarios presented in this section. Firstly, Test 2 is evaluated by comparing the maximum far-field temperatures with both numerical models, with and without the cable. As can be seen in Table 5, and as previously commented, the smaller severity of the whirls imply that the temperatures are only slightly underpredicted, with a maximum errror of 7.8%.

The influence of the HRR nominal value is numerically assessed by a qualitative comparison between two additional numerical models that do not include the cable, i.e. 3.5 MW and 5 MW. Firstly, fire whirls are predicted in the four numerical scenarios but the formation frequency varies for every case due to the high flame instabilities observed. The tangential velocity fields and the temperature core radii are analysed for 1.54 MW (Fig. 11a–c), 2.66 MW (Fig. 11d–f), 3.5 MW (Fig. 11g–i), and 5 MW (Fig. 11j-l). As can be observed, at the lowest heights of 0.4 and 2.4 m (Fig. 11a–b, d.-e, g-h, j-k), for some time instants, there are no significant differences in the values of maximum circulation. At the height of 4.4 m, the maximum circulation slightly decreases, except for the case with the maximum HRR, that remains nearly constant. It is important to note that these numerical whirls are very unstable and the numerical values highly differ during their evolution. In the same way, except for the case of 5 MW, the temperature core radii increase with height. As the HRR grows, the size of the whirls increases and their inclination and deviation from the pan centre are more relevant, particularly for the maximum HRR. In addition, the total maximum flame heights can be qualitatively defined from the temperature fields. As it was observed in the experiments, the total flame heights did not show a substantial elongation, then being classified as medium scale fire whirls, i.e. from 1 to 10 m [34]. In that way, the numerical models of Test 1 and Test 2 behave similarly to the experiments. Thus, considering the temperature fields, with 550 °C as the maximum temperature of the flaming region as in Ref. [25], the flame heights can be qualitatively obtained as: 4.5 m, 5.0 m, 7 m and 7.5 m for 1.54 MW, 2.66 MW, 3.5 and 5 MW respectively. It important to note how the flame height is in accordance with the experimental observations from both Tests. For Test 1, even though the flame height could not be experimentally measured with enough precision, the results can be considered slightly underpredicted. For Test 2, the numerical results are very close to the observed values.

4. Conclusions

The spontaneous generation and evolution of fire whirls in two full-scale atrium experiments, with time-averaged heat release rate values of 1.54 MW and 2.66 MW are presented. The tests were carried out with a mechanical exhaust of 18.32 m^3/s and an asymmetric layout of distant inlet vents, as in a fixed frame facility. Above the pool fires, a horizontal cable was used to locate the thermocouples and was observed to impact the swirling flames.

Numerical models with FDS 6.7.5. have been performed to reproduce the temperature both in the near and the far fields. Two types of input for the heat release rate have been assessed: the measured experimental curve and a time-averaged value. In addition, two numerical models of the atrium have been generated, i. e., with and without the mentioned cable. The major findings of the present work are summarized as follows:

- With both types of heat release rate inputs, fire whirls are numerically predicted. Circulation is well predicted, and the Burgers vortex model is followed. The obtained temperatures can distinguish between the continuous flame and plume regions. However, this is only possible with element sizes of 0.1 m and 0.05 m for the flame region.
- When introducing the real HRR curve as an input to the models, fire whirls are not reproduced in the same instants as expected. The temperatures in the far-field are very well predicted, but the number of whirls is reduced compared to the experiments.
- The time-averaged HRR curve reproduces a higher number of whirls, particularly when the cable is introduced. However, a higher discrepancy in the far-field temperatures is obtained, with a maximum of 17.7%, mainly due to the smaller value of HRR. In this case, the finest grid ($\Delta = 0.05$ m) is required to fairly reproduce the observed height of the whirls, despite its relevant difference in the periodicity of their formation and slight discrepancies in the far-field temperature values. An optimum element size of 0.01 m is suggested for this HRR, although the heights of the fire whirls are underpredicted.
- The introduction of small obstacles near the flame clearly affects the transient results, which might be relevant when considering possible fire spread mechanisms. However, the consideration of these more complex numerical models implies a substantial increase in the computational cost of the numerical models.
- The numerical models capture the influence of the HRR nominal value, mainly in the flame height. In the range tested, the numerical results show good agreement with the observed range of flame heights, without any noticed significant elongation.

Fire whirls can be generated indoors like in vertical shafts of tall buildings, atria with mechanical ventilation, or even spaces with venting conditions considered in the current regulations. It is then relevant to highlight how these swirling flames may enhance propagation and produce devastating damage if they are not considered during the fire safety design process.

Author statement

Alexis Cantizano (Corresponding Author): Conceptualization, Methodology, Software, Investigation, Formal Analysis, Writing - Original Draft; **Pablo Ayala:** Methodology, Software, Investigation, Formal analysis, Writing - Original Draft; **Eva Arenas:** Formal analysis, Investigation, Writing - Review & Editing; **José Rubén Pérez:** Investigation, Writing - Review & Editing; **Cándido Gutiérrez-Montes**: Software, Investigation, Validation, Writing - Review & Editing.

Table 5
Maximum temperatures in the far-field (Test 2).

Height		Temperature (°C)/Error (%)	
		Exp.	$\Delta = 0.1$
7.5 m	No cable	60.9	62.6/2.8
	Cable		63.3/4.0
15 m	No cable	73.6	67.9/7.8
	Cable		69.4/5.8

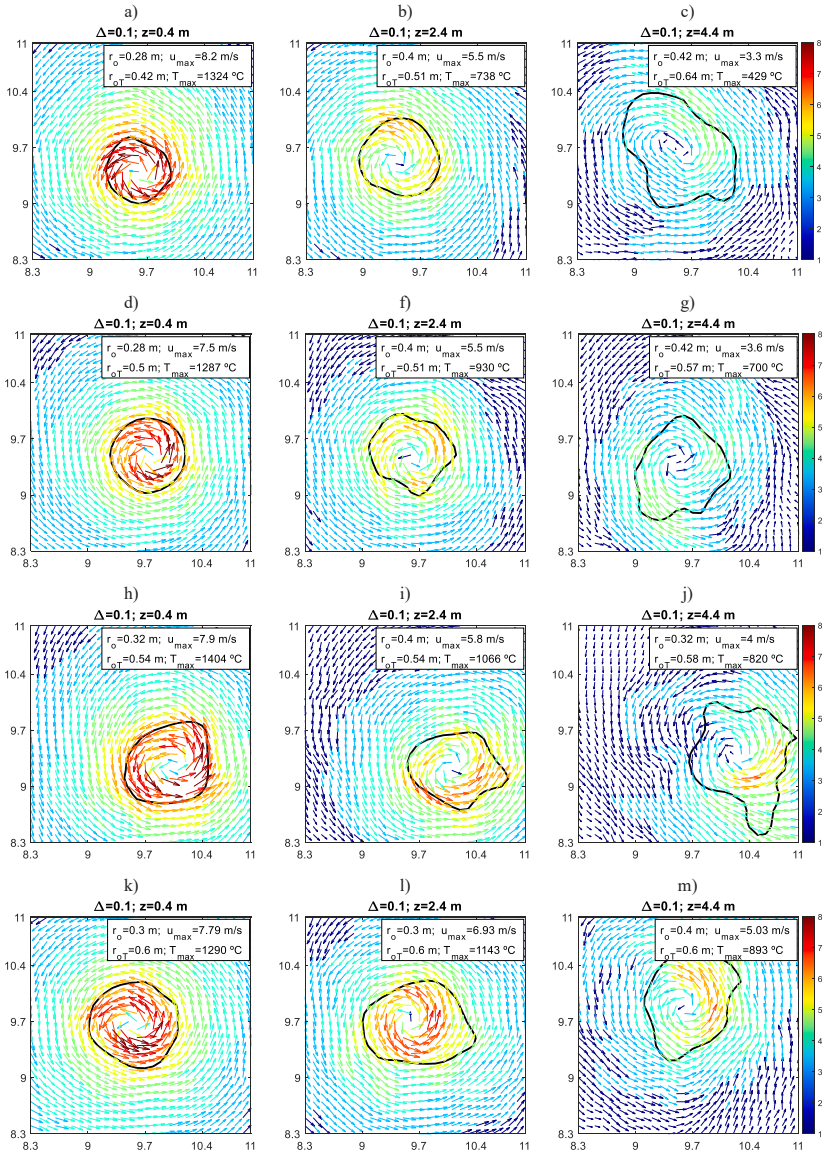

Fig. 11. Tangential velocity fields and temperature core radii.

Declaration of competing interest

The authors declare that they have no known competing financial interests or personal relationships that could have appeared to influence the work reported in this paper.

Data availability

Data will be made available on request.

Appendix A. Supplementary data

Supplementary data to this article can be found online at https://doi.org/10.1016/j.csite.2022.102513.

References

[1] C. Wang, A.C.Y. Yuen, Q.N. Chan, T.B.Y. Chen, H.L. Yip, S.C.-P. Cheung, S. Kook, G.H. Yeoh, Numerical study of the comparison of symmetrical and asymmetrical eddy-generation scheme on the fire whirl formulation and evolution, Appl. Sci. 10 (2020) 318, https://doi.org/10.3390/app10010318.
[2] J. Lei, N. Liu, K. Satoh, Buoyant pool fires under imposed circulations before the formation of fire whirls, Proc. Combust. Inst. 35 (2015) 2503–2510.
[3] P.B. Dermer, A.Y. Varaksin, A.I. Leontiev, The wall-free non-stationary fire whirls generation by axisymmetric burning of solid fuel pellets, Int. J. Heat Mass Tran. 110 (2017) 890–897, https://doi.org/10.1016/j.ijheatmasstransfer.2017.03.076.
[4] K.A. Hartl, A.J. Smits, Scaling of a small scale burner fire whirl, Combust. Flame 163 (2016) 202–208, https://doi.org/10.1016/j.combustflame.2015.09.027.
[5] K. Kuwana, K. Sekimoto, T. Minami, T. Tashiro, K. Saito, Scale-model experiments of moving fire whirl over a line fire, Proc. Combust. Inst. 34 (2013) 2625–2631.
[6] J. Lei, N. Liu, R. Tu, Flame height of turbulent fire whirls: a model study by concept of turbulence suppression, Proc. Combust. Inst. 36 (2017) 3131–3138, https://doi.org/10.1016/j.proci.2016.06.080.
[7] J. Lei, N. Liu, L. Zhang, H. Chen, L. Shu, P. Chen, Z. Deng, J. Zhu, K. Satoh, J.L. de Ris, Experimental research on combustion dynamics of medium-scale fire whirl, Proc. Combust. Inst. 33 (2011) 2407–2415.
[8] K. Satoh, K.-T. Yang, Experimental observations of swirling fires, ASME-PUBLICATIONS-HTD. 335 (1996) 393–400.
[9] P. Wang, N. Liu, Y. Bai, L. Zhang, K. Satoh, X. Liu, P. Wang, N. Liu, Y. Bai, L. Zhang, K. Satoh, X. Liu, An experimental study on thermal radiation of fire whirl, Int. J. Wildland Fire 26 (2017) 693–705, https://doi.org/10.1071/WF17010.
[10] Y. Yan, X. Fang, S.C.P. Cheung, P. Yan, J. Tu, Characterisation and analysis on the instantaneous development and dynamic vortex cores of fire whirls in a fixed-frame facility, Int. J. Heat Mass Tran. 175 (2021), 121355, https://doi.org/10.1016/j.ijheatmasstransfer.2021.121355.
[11] K. Zhou, N. Liu, J.S. Lozano, Y. Shan, B. Yao, K. Satoh, Effect of flow circulation on combustion dynamics of fire whirl, Proc. Combust. Inst. 34 (2013) 2617–2624.
[12] K.H. Chuah, K. Kuwana, K. Saito, Modeling a fire whirl generated over a 5-cm-diameter methanol pool fire, Combust. Flame 156 (2009) 1828–1833.
[13] K.H. Chuah, G. Kushida, The prediction of flame heights and flame shapes of small fire whirls, Proc. Combust. Inst. 31 (2007) 2599–2606.
[14] J. Lei, C. Ji, N. Liu, L. Zhang, Effect of imposed circulation on temperature and velocity in general fire whirl: an experimental investigation, Proc. Combust. Inst. 37 (2019) 4295–4302, https://doi.org/10.1016/j.proci.2018.06.055.
[15] J. Lei, N. Liu, Reciprocal transitions between buoyant diffusion flame and fire whirl, Combust. Flame 167 (2016) 463–471, https://doi.org/10.1016/j.combustflame.2015.10.009.
[16] P. Wang, N. Liu, K. Hartl, A. Smits, Measurement of the flow field of fire whirl, Fire Technol. 52 (2016) 263–272.
[17] H.W. Emmons, S.-J. Ying, The fire whirl, Symposium (International) on Combustion 11 (1967) 475–488, https://doi.org/10.1016/S0082-0784(67)80172-3.
[18] F. Battaglia, K. Mcgrattan, R. Rehm, H. Baum, Simulating fire whirls, Combust. Theor. Model. 4 (2000) 123–138, https://doi.org/10.1088/1364-7830/4/2/303.
[19] R.N. Meroney, Fire whirls and building aerodynamics, in: Proceedings of the 11th International Conference on Wind Engineering, Citeseer, 2003.
[20] A.Yu Snegirev, J.A. Marsden, J. Francis, G.M. Makhviladze, Numerical studies and experimental observations of whirling flames, Int. J. Heat Mass Tran. 47 (2004) 2523–2539, https://doi.org/10.1016/j.ijheatmasstransfer.2004.02.002.
[21] J. Lei, N. Liu, Flame precession of fire whirls: a further experimental study, Fire Saf. J. 79 (2016) 1–9, https://doi.org/10.1016/j.firesaf.2015.10.005.
[22] R. Zhou, Z.-N. Wu, Fire whirls due to surrounding flame sources and the influence of the rotation speed on the flame height, J. Fluid Mech. 583 (2007) 313–345.
[23] R. Zhou, Applications of the equivalent gap fraction criterion method for fire whirl risk evaluation and prevention in a real fire disaster, Fire Technol. 50 (2014) 143–159, https://doi.org/10.1007/s10694-012-0277-6.
[24] W.K. Chow, J.F. Dang, Y. Gao, C.L. Chow, Dependence of flame height of internal fire whirl in a vertical shaft on fuel burning rate in pool fire, Appl. Therm. Eng. 121 (2017) 712–720, https://doi.org/10.1016/j.applthermaleng.2017.04.108.
[25] Z. Gao, S.S. Li, Y. Gao, H.Y. Hung, W. Chow, Numerical studies on swirling of internal fire whirls with experimental justifications, Build. Simulat. 14 (2021) 1499–1509, https://doi.org/10.1007/s12273-020-0756-5.
[26] G.W. Zou, H.Y. Hung, W.K. Chow, A study of correlation between flame height and gap width of an internal fire whirl in a vertical shaft with a single corner gap, Indoor Built Environ. 28 (2019) 34–45, https://doi.org/10.1177/1420326X17729742.
[27] C. Gutiérrez-Montes, E. Sanmiguel-Rojas, A. Viedma, G. Rein, Experimental data and numerical modelling of 1.3 and 2.3 MW fires in a 20 m cubic atrium, Build. Environ. 44 (2009) 1827–1839, https://doi.org/10.1016/j.buildenv.2008.12.010.
[28] P. Ayala, A. Cantizano, G. Rein, G. Vigne, C. Gutiérrez-Montes, Fire experiments and simulations in a full-scale Atrium under transient and asymmetric venting conditions, Fire Technol. 52 (2015) 51–78, https://doi.org/10.1007/s10694-015-0487-9.
[29] G. Vigne, W. Węgrzyński, A. Cantizano, P. Ayala, G. Rein, C. Gutiérrez-Montes, Experimental and computational study of smoke dynamics from multiple fire sources inside a large-volume building, Build. Simulat. 14 (2021) 1147–1161, https://doi.org/10.1007/s12273-020-0715-1.
[30] K. McGrattan, R. McDermott, S. Hostikka, J. Floyd, FDS (Version 6) User's Guide, Technical Report, NIST, 2013.
[31] M.J. Hurley, D.T. Gottuk, J.R. Hall Jr., K. Harada, E.D. Kuligowski, M. Puchovsky, J.M. Watts Jr., C.J. Wieczorek, SFPE Handbook of Fire Protection Engineering, Springer, 2015 others, https://books.google.es/books?hl=es&lr=&id=xP2zCgAAQBAJ&oi=fnd&pg=PR7&dq=handbook+of+science+protection+engineers&ots=1_4mB4HDXs&sig=5bSGFVcV2_wkbX9agNidTBem9Vg.
[32] P. Ayala, A. Cantizano, G. Rein, C. Gutiérrez-Montes, Factors affecting the make-up air and their influence on the dynamics of atrium fires, Fire Technol. 54 (2018) 1067–1091.
[33] R. Dobashi, T. Okura, R. Nagaoka, Y. Hayashi, T. Mogi, Experimental study on flame height and radiant heat of fire whirls, Fire Technol. 52 (2016) 1069–1080.
[34] A. Tohidi, M.J. Gollner, H. Xiao, Fire whirls, Annu. Rev. Fluid Mech. 50 (2018) 187–213, https://doi.org/10.1146/annurev-fluid-122316-045209.
[35] J. Lei, N. Liu, L. Zhang, K. Satoh, Temperature, velocity and air entrainment of fire whirl plume: a comprehensive experimental investigation, Combust. Flame 162 (2015) 745–758, https://doi.org/10.1016/j.combustflame.2014.08.017.
[36] P. Ayala, A. Cantizano, E.F. Sánchez-Úbeda, C. Gutiérrez-Montes, The use of fractional factorial design for atrium fires prediction, Fire Technol. 53 (2017) 893–916, https://doi.org/10.1007/s10694-016-0609-z.
[37] S. Hostikka, M. Kokkala, J. Vaari, Experimental Study of the Localized Room Fires NFSC2 Test Series, VTT TIEDOTTEITA, 2001.